

Identification of novel fluorescent probes preventing PrP(Sc) replication in prion diseases

This is the peer reviewed version of the following article:

Original:

Zaccagnini, L., Brogi, S., Brindisi, M., Gemma, S., Chemi, G., Legname, G., et al. (2017). Identification of novel fluorescent probes preventing PrP(Sc) replication in prion diseases. EUROPEAN JOURNAL OF MEDICINAL CHEMISTRY, 127, 859-873 [10.1016/j.ejmech.2016.10.064].

Availability:

This version is available <http://hdl.handle.net/11365/999896> since 2017-05-25T10:55:18Z

Published:

DOI: <http://doi.org/10.1016/j.ejmech.2016.10.064>

Terms of use:

Open Access

The terms and conditions for the reuse of this version of the manuscript are specified in the publishing policy. Works made available under a Creative Commons license can be used according to the terms and conditions of said license.

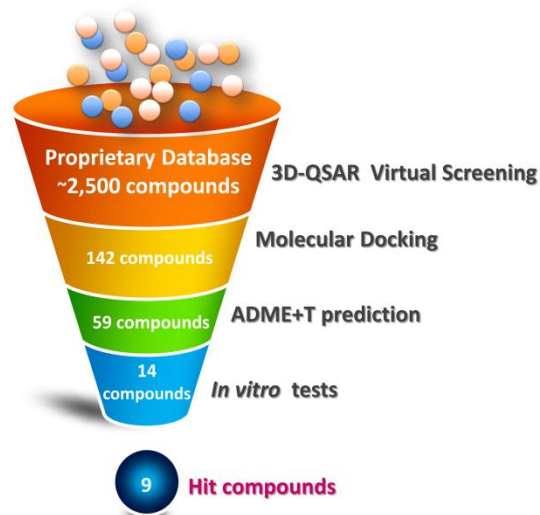
For all terms of use and more information see the publisher's website.

(Article begins on next page)

Graphical Abstract

Identification of Novel Fluorescent Probes Preventing PrP^{Sc} Replication in Prion Diseases

Screening workflow



Highlights

- A 3D-QSAR model was generated for the prediction of anti-prion activity
- The model was used in virtual screening protocol coupled with molecular docking on PrP^C
- Evaluation of cell viability on ScN2a highlighted the non-toxic profile of our retrieved hits
- Nine out of eleven selected compounds showed in vitro anti-prion activity
- Compound **96** is a promising hit interfering with pathological transition of PrP^C to PrP^{Sc}
- **96** displays a fluorescence staining profile suggesting its application as a diagnostic for TSE

Identification of Novel Fluorescent Probes Preventing PrP^{Sc} Replication in Prion Diseases

Ludovica Zaccagnini^{a,1}, Simone Brogi^{b,c,1}, Margherita Brindisi^{b,c}, Sandra Gemma^{*,b,c}, Giulia Chemi^{b,c},
Giuseppe Legname^{**a}, Giuseppe Campiani^{b,c}, Stefania Butini^{b,c}

^aLaboratory of Prion Biology, Department of Neuroscience, Scuola Internazionale Superiore di Studi Avanzati (SISSA), via Bonomea 265, 34136 Trieste, Italy.

^bEuropean Research Centre for Drug Discovery and Development (NatSynDrugs), Università degli Studi di Siena, via Aldo Moro 2, 53100 Siena, Italy

^cDipartimento di Biotecnologie, Chimica e Farmacia, Università degli Studi di Siena, via Aldo Moro 2, 53100 Siena, Italy

Authors for correspondence:

*Sandra Gemma Tel.: +39-0577-234326; fax: +39-0577-23234254; e-mail: gemma@unisi.it;

**Giuseppe Legname Tel.: +39-040-3787715; fax: +39-040-3787702; e-mail: legname@sissa.it

¹These authors contributed equally to this work.

Keywords: Pharmacophore Modeling, 3D-QSAR, Prion, anti-prion agents, theranostic tools

ABSTRACT

Prion diseases are serious, not curable neurodegenerative disorders caused by the accumulation of the misfolded protein PrP^{Sc} that represents the pathological variant of the normally folded cellular protein PrP^C. Molecules that binds the cellular isoform PrP^C preventing its misfolding, could arrest the progression of pathological conditions related to the abnormal PrP protein. In this context, by combining 3D-QSAR model, derived from pharmacophore-based alignment, with molecular docking procedure and physico-chemical properties prediction we have developed a virtual screening protocol to find novel chemicals able to prevent PrP^C misfolding. We identified different hits characterized by low toxicity and able to inhibit PrP^{Sc} accumulation in vitro in prion-infected neuroblastoma cell lines (ScN2a). In this assay, the pyrroloquinoxaline hydrazone **96** showed the higher potency with an IC₅₀ value of 1.6 μM. Pyrroloquinoxaline **96** was demonstrated also to bind PrP^{Sc} aggregates in infected ScN2a cells with a fluorescence pattern comparable to that found for Thioflavin-T. In consideration of its satisfactory physico-chemical properties, including predicted blood brain barrier permeability, **96** could represent an interesting prototypic hit for the development of diagnostic and therapeutic probes for prion diseases.

1. Introduction

Transmissible spongiform encephalopathies (TSE), commonly known as prion diseases, are a rare and fatal group of neuropathies hallmarked by abnormal prion protein accumulation in the brain, spongiform vacuolation, and severe neuronal loss [1, 2]. These disorders include Creutzfeldt-Jakob disease, fatal familial insomnia, Gerstmann-Sträussler-Scheinker syndrome, and kuru in humans, bovine spongiform encephalopathy in cattle, scrapie in sheep and goats, and chronic wasting disease in cervids [3]. Their unique etiologic agent is an abnormal, misfolded form of the cellular prion protein (PrP^C), denominated scrapie PrP (PrP^{Sc}) [3]. It is well-established that the tertiary structure of PrP^C is

rich in α -helix motif, and typically anchored through a C-terminal moiety of glycosylphosphatidylinositol (GPI) to the cellular surface, highly conserved among mammals [4]. On the contrary, PrP^{Sc} is rich in β -sheet motif and tends to form aggregates [5, 6]. In human or animal diseases the misfolding event causes a self-aggregation and polymerization of the protein with the formation of deposits of insoluble amyloidogenic fibrils [7]. The final neuronal damage, leading to brain dysfunction, including motor and cognitive impairment, and dementia is mediated by several mechanisms, which are triggered by protein accumulation [4, 8]. Thus, prion diseases are a prototypical example of protein misfolding disorders or conformational disorders (PCD), which also include Alzheimer's disease, Parkinson's disease, Huntington's disease, and amyotrophic lateral sclerosis [9, 10]. All these pathologies are commonly characterized by an incorrect folding of cellular proteins showing altered tertiary structures with respect to native structures.

Although the physiological function of PrP^C still remains controversial, as well as the molecular mechanisms leading to its misfolding [4, 11-14], preventing or reducing the rate of PrP^{Sc} conversion is currently the most widely applied therapeutic strategy against prion diseases [15-17]. Accordingly, a number of molecules which act by directly binding PrP^C and/or blocking the conversion from PrP^C to PrP^{Sc} have been discovered by applying medicinal chemistry [18-26] and *in silico* methods [27-29] including repurposing strategies [30] and multi-targeting approaches [31]. Despite these efforts, effective therapies to treat prion diseases are still missing [22, 32-35]. Moreover, diagnostic tests, which to date consist in electroencephalogram, magnetic resonance imaging, detection of 14-3-3 protein in cerebral spinal fluid, positron emission tomography [36], Protein Misfolding Cyclic Amplification [37] and Real-time Quaking-Induced Conversion [38], do not allow early diagnosis [39].

To discover novel effective drugs and diagnostic tools, the exploitation of *in silico* methodologies can represent a valuable mean for detecting molecules able to inhibit the PrP^{Sc} formation [27-29]. In particular, we herein report a virtual screening protocol, based on a three-dimensional quantitative

structure-activity relationship (3D-QSAR) model coupled with molecular docking, to find novel tools able to prevent PrP^C misfolding. Moreover, prediction of physico-chemical parameters, including cell membrane and BBB permeability, has been considered to select the hit compounds with potential anti-prion activity. The 3D-QSAR model was generated by using Phase software and virtual screening methodology [40-46]. Cell toxicity and anti-prion activity were subsequently assessed. The employed screening workflow that has allowed us to identify compounds with low toxicity and remarkable anti-prion activity is depicted in Figure 1.

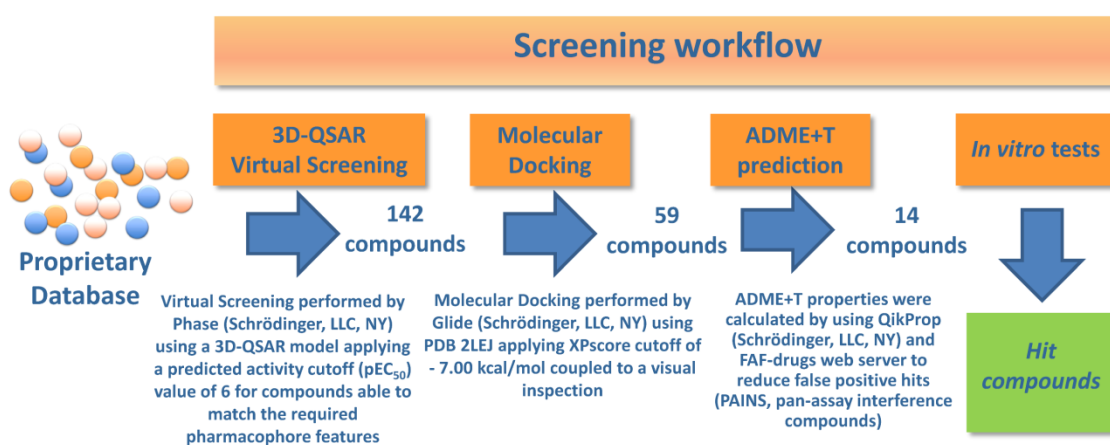


Figure 1. Computational protocol employed in this study.

The most promising hit (namely, compound **96**) was not only able to interfere with PrP^{Sc}, but was also able to stain PrP^{Sc} aggregates in infected ScN2a cells with a fluorescence staining pattern comparable to that found for the amyloid dye Thioflavin-T (ThT). This peculiar profile makes our hit a suitable diagnostic tool for prion diseases with a concomitant therapeutic potential (inhibition of PrP^{Sc} accumulation in cells).

2. Materials and Methods

2.1. Computational Details

2.1.1. Ligands and database preparation

The 3D structure of all the molecules used in Phase was built in Maestro. For the sake of clarity for the molecules possessing known stereochemistry, the absolute configuration was specified during the drawing of the compounds. Our proprietary database was built in Maestro suite. All the structures (ligands for developing the 3D-QSAR model and the structures of our proprietary database) were minimized by means of MacroModel (MacroModel, version 9.9, Schrödinger, LLC, New York, NY, 2011) using the OPLSAA_2005 as force field [47]. GB/SA model was used in order to simulate the solvent effect applying “no cutoff” for non-bonded interactions. PRCG method (2000 maximum iterations and 0.001 gradient convergence threshold) was employed. Compounds were then submitted to LigPrep program (version 2.5, Schrödinger, LLC, New York, NY, 2011), producing a possible ionization state taking also into account all enantiomers and tautomers at $\text{pH } 7.0 \pm 0.5$.

Concerning the ligands used for developing 3D-QSAR model an exhaustive conformational analysis was carried out by means of MacroModel (MacroModel, version 9.9, Schrödinger, LLC, New York, NY, 2011) after the minimization above reported. The conformational searches were carried out by application of the MCMM (Monte Carlo Multiple Minimum) torsional sampling method, performing automatic setup with 21 kJ/mol (5.02 kcal/ mol) in the energy window for saving structure and a 0.5 Å cutoff distance for redundant conformers.

2.1.2. Protein preparation

The three-dimensional structure of the human PrP^C was taken from Protein Data Bank (PDB ID 2LEJ), imported into Maestro suite 2011 and submitted to protein preparation wizard to obtain a reasonable starting structure for docking calculation.

2.1.3. 3D-QSAR model generation and validation

Phase (Phase, version 3.3, Schrödinger, LLC, New York, NY, 2011), implemented in Maestro modeling package, was used to generate pharmacophore and 3D-QSAR model for the prediction of anti-prion activity. The 3D structure of all the molecules used in Phase was built in Maestro as reported in “Ligands and database preparation” section. The program, given a set of molecules with activity, utilizes fine-grained conformational sampling and a range of scoring techniques to identify a common pharmacophore hypothesis, which conveys characteristics of 3D chemical structures that are purported to be critical for the activity. Pharmacophore feature sites for the molecules were assigned using a set of features defined in Phase as hydrogen-bond acceptor (A), hydrogen-bond donor (D), hydrophobic group (H), negatively charged group (N), positively charged group (P), and aromatic ring (R). Nine highly active compounds possessing anti-prion properties preventing misfolding (**14**, **27**, **33**, **34**, **51-53**, **57**, **58**; Table 1) were selected for generating the pharmacophore hypotheses. Common features pharmacophore hypotheses were identified, scored and ranked using conformational analysis and a tree-based partitioning technique. The best-ranked pharmacophore model obtained by Phase (AARRR.20, shown in Figure 2 superimposed to **33**), consisted of five features: three aromatic rings (R_1 , R_2 and R_3) and two hydrogen-bond acceptors (A_1 and A_2). The inter-features distances were measured by using the site measurements tool implemented in Phase. This pharmacophore was chosen for further 3D-QSAR analysis. All molecules used for QSAR studies (Table 1) were aligned to the selected pharmacophore hypothesis. In this study, we set a pEC_{50} threshold for the selection of active and inactive PrP^C ligands. In particular, compounds that showed an EC_{50} over 10 μM were considered as inactive compounds. Weak inhibitors were considered compounds with EC_{50} between 300 nM and 10 μM , while compounds that possess an $EC_{50} < 300$ nM were considered potent inhibitors of misfolding and consequently as active during 3D-QSAR model generation. Notably, we have considered only the compounds with experimentally defined inhibitory activity to avoid potential mistakes arising from the inclusion in the set of compounds with undetermined activity. Atom-based

QSAR models were generated for AARRR.20 hypothesis using the 35-member training set (58 compounds were randomly divided: 60% in the training set and 40% in the test set) and a grid spacing of 1.0 Å. QSAR models containing one to five PLS factors were generated, and cross validation was performed using leave-n-out (LnO) method as specified in Phase user manual. All graphics were generated by means of Maestro (Maestro, version 9.2, Schrödinger, LLC, New York, NY, 2011).

Database of Useful Decoys: Enhanced (DUD-E) web server (<http://dude.docking.org> access date January 2016) was used to generate a set of decoys starting from 26 active compounds as discussed in the main text. For the active ligands DUD-E server provided 1550 inactive ligands (redundant structures in the output files were deleted) from a subset of the ZINC database (<http://zinc.docking.org/> access date January 2016) filtered using the Lipinski rules for drug-likeness, for a total of 1576 compounds between active and inactive. Each of these inactive decoys was chosen to resemble the reference ligand physico-chemical properties but to have different 2D structure (e. g. very large difference of Tanimoto coefficient between active molecules and decoys). After the generation, the decoys sets were downloaded as smiles files and imported into Maestro and submitted to LigPrep application to correctly prepare the 3D structures as well as for removing potential erroneous structures. A single file containing active molecules and decoys was created and submitted to Phase for predicting the activity of the database by applying the developed 3D-QSAR model. After decoys generation and activity evaluation, enrichment factor (*EF*) value, Güner and Henry score, i. e. goodness of hit score (*GH*) were calculated by the equations 1 and 2, respectively.

$$EF = \frac{Ha/Ht}{(A/D)} \quad \text{eq. (1)}$$

$$GH = \left\{ \frac{[Ha * (3A + Ht)]}{4HtA} \right\} * \left[1 - \frac{(Ht - Ha)}{(D - A)} \right] \quad \text{eq. (2)}$$

where Ht is the total number of molecules in the hit list found by virtual screening, Ha represents the total active molecules found by screening applying the mentioned cutoff value, A is the total of the active molecules present in the database, while D is the total molecules present in the set. The range of GH score varies from 0 to 1. GH score 0 means a null model, while the GH score 1 means generation of an ideal model. Moreover, also the % yield of actives (%YA) and % ratio of actives (%RA) were evaluated by the equations 3 and 4, respectively.

$$\%YA = \left[\left(\frac{Ha}{Ht} \right) * 100 \right] \quad \text{eq. (3)}$$

$$\%RA = \left[\left(\frac{Ha}{A} \right) * 100 \right] \quad \text{eq. (4)}$$

Moreover, to evaluate the performance of the 3D-QSAR model a Receiving Operator Curve (ROC) [48] was employed. For this purpose we have adopted a script downloaded from Schrödinger website (<http://www.schrodinger.com/> access date January 2016) namely Enrichment Calculator (*enrichment.py*). This script is able to calculate the enrichment metrics from virtual screening calculations using the output structure file and a list of known actives, including area under the receiver-operating characteristic curve (AUC). The virtual screening procedure, using active molecules and decoys and presented in the *in silico* validation paragraph, provided a ranking of compounds from the top-predicted molecules. This ranking data coupled to a list file of active molecules was submitted to the mentioned application. The output is reported in Figure 4.

2.1.4. Molecular Docking

Molecular Docking was carried out by Glide (Grid-Based Ligand Docking with Energetics) using the ligands and the protein prepared as above-mentioned, applying Glide extra precision (XP) method [49, 50]. Energy grid was prepared using default value of protein atom scaling factor (1.0 Å) within a cubic box centered on H187 that can represent the center of the D-pocket (residues 156-162 and 180-210 in

human PrP^C). After grid generation, the ligands and the crystallized inhibitor were docked into the enzymes with default parameters (no constraints were added). The number of poses entered to post-docking minimization was set to 50. Glide XP score was evaluated. The interactions of compounds with PrP^C were assessed by using ligand-interaction diagram and a script for displaying hydrophobic interactions (*display_hydrophobic_interactions.py*) downloaded from Schrödinger website and implemented in Maestro.

2.1.5. Molecular properties prediction

Physico-chemical properties were evaluated by means of QikProp (QikProp, version 3.4, Schrödinger, LLC, New York, NY, 2011), while the assessment for potential PAINS in the set of selected molecules was conducted by means of FAFDrugs3.0 (<http://www.fafdrugs3.mti.univ-paris-diderot.fr> access date January 2016).

2.2. Biological Evaluation

2.2.1. Cell Culture

Mouse neuroblastoma cells chronically infected with the Rocky Mountain Laboratory (RML) prion strain (ScN2a) were grown in Minimal Essential Medium (MEM) supplemented with 10% fetal bovine serum (FBS), 1% non-essential amino acids (NEAA), 1% L-glutamax and 1% penicillin-streptomycin. Non-infected N2a cells were used as control. Immortalized mouse hypothalamic (GT1) and chronically infected ScGT1 cells were grown in Dulbecco's modified Eagle's medium (DMEM) supplemented with 10% FBS and 1% penicillin-streptomycin. All cell lines were maintained at 37 °C under 5% CO₂.

2.2.2. Compounds

Compounds, selected following the above mentioned computational protocol, were retrieved from our stockroom. The syntheses of identified compounds (**89-92** and **95-104**; Supplementary Table 3) were carried out as already reported [51-56]. The newly disclosed compounds **93** and **94** were prepared

following the previously described synthetic protocol [56] and spectroscopic data are reported in the Supplementary Information.

All the compounds were dissolved in 100% dimethyl sulfoxide (DMSO), to a 10 mM stock solution, and compounds **93** and **104** to a 20 mM stock solution. From these stock solutions, intermediate dilutions were prepared as needed. For cell treatment, stock solutions were further diluted in 100% Ethanol (EtOH) to a final concentration of 1 mM. Each compound was then diluted in cell culture medium. In the cell medium, the final concentration of DMSO was never above 0.1%. Detailed treatment conditions are provided in following methods. Mock controls were treated with vehicle only under the same conditions.

2.2.3. Assessment of cell viability (MTT assay)

N2a, ScN2a, GT1 and ScGT1 cells, were maintained in culture and grown to 80% confluence. The medium was changed and the cells were detached. The cell density was determined by cell counting using Scepter™ 2.0 Cell Counter (Millipore). The cell density was adjusted to 2.5×10^4 cell/mL with MEM (N2a, ScN2a) or 3×10^4 with DMEM (GT1, ScGT1). The cell suspension was added to each well of a 96-well, tissue culture-treated, clear bottom, plate (Costar) and the cells were allowed to settle for 2 hours at 37 °C under 5% CO₂ prior to the addition of the compounds. Each compound (dissolved in EtOH) was diluted in the cell medium to a final concentration of 0.1, 1 and 10 µM. After 2 h, cell culture medium was removed and replaced by compound-containing medium. The plate was incubated at 37 °C under 5% CO₂ for 5 days (N2a, ScN2a) or 7 days (GT1, ScGT1). The 3-(4,5-dimethylthiazol-2-yl)-2,5-diphenyltetrazolium bromide (MTT, SIGMA) was diluted in phosphate buffer solution (PBS) to a working dilution of 5 mg/mL. The medium was then removed and the cells were incubated with the MTT solution for 3 hours at 37 °C under 5% CO₂. After incubation, a solution of DMSO/2-Propanol (1:1) was added to each well and the plate was kept at room temperature (RT) for 30 minutes

before reading. The emission intensity was quantified using a Spectramax Gemini EM (SoftMax Pro) plate reader, excitation/emission ratio equal to 570/690 nm. MTT assays were performed in triplicate.

2.2.4. PrP^{Sc} detection in cell lysates by Western Blotting

The amount of PK-resistant PrP^{Sc} was measured in ScN2a and ScGT1 treated with 0.1, 1 and 10 μ M concentration of each compound. After 5 days (ScN2a) or 7 days (ScGT1) of treatment, the accumulation of PrP protein was detected by immunoblotting of lysed cells before and after PK digestion.

Cell lysates. After removing the medium and washing the cells with PBS, 500 μ L of lysis buffer (10 mM Tris-HCl pH 8.0, 150 mM NaCl, 0.5 % nonidet P-40, 0.5 % deoxycholic acid sodium salt) were added to the cell plates, then the lysates were collected and pelleted by centrifugation at 2000 rpm for 10 minutes at 4 °C in a bench microfuge (Eppendorf). The supernatants were collected and the total protein concentration was measured using bicinchoninic acid assay (Pierce).

PK digestion. 500 μ g of protein were digested with 10 μ g of PK (Roche) for 1 hour at 37 °C. The reaction was arrested with 2 mM of phenylmethanesulphonylfluoride (PMSF, SIGMA) and the PK-digested cell lysates were centrifuged at 55,000 rpm for 75 minutes at 4 °C in an ultracentrifuge (Beckman Coulter). After the centrifugation, the supernatants were discarded and the pellets were re-suspended in 2X sample loading buffer (125 mM Tris HCl, pH 6.8, 10% 2-mercapethanol, 4% SDS, 0.2% bromophenol blue, 20% glycerol) and boiled for 20 minutes at 100 °C. An amount equal to 50 μ g of total proteins was used for the non-PK-digested samples, boiled for 5 minutes.

SDS page assay and immunoblotting. Samples were loaded onto a 12% Tris-Glycine SDS-PAGE gel for protein separation, then they were transferred to a nitrocellulose membrane (GE Healthcare). The membrane was blocked with 5% non-fat milk in TBST (Tris 200 mM, NaCl 1.5 mM, 1% Tween-20) for 1 hour at RT and incubated with 1 μ g/mL anti-PrP Fab W226, diluted in blocking solution,

overnight at 4 °C. After three washes with TBST, the membrane was incubated for 1 hour at RT with secondary antibody (goat anti-mouse IgG F(Ab)₂ conjugated with horseradish peroxidase (HRP), DAKO) diluted 1:2000 in blocking solution. After several washes, the signal was detected using enhanced chemiluminescent system (ECL, Amersham Biosciences) and Uvitec Alliance (Cambridge). Densitometric analysis was performed using Uviband Analysis Software. Data are expressed as mean \pm SD, and the values of the controls are adjusted to 1. Each experiment was performed in triplicate.

2.2.5. PrP^C detection in cell lysates by Western Blotting

The same treatment conditions reported above were used for non-infected N2a and GT1 cells. After 5 days (N2a) or 7 days (GT1) of drug treatment, the amount of PrP^C was measured by immunoblotting of lysed cells. 50 μ g of total proteins were used for the analysis. Same protocol as above was used, without PK digestion step. Each experiment was performed in triplicate.

2.2.6. PrP^{Sc} quantification by ELISA

PK digestion of cell lysates was performed as described above. After ultracentrifugation, pellets were dissolved and denatured in 50 μ L of 8 M guanidine hydrochloride (GdnHCl) in coating buffer (0.1 M sodium bicarbonate, pH 8.2) for 1 hour and diluted into 500 μ L of coating buffer. 20 μ L of the suspension were transferred to 96-well MaxiSorp ELISA plates (Nunc), with each well containing 180 μ L coating buffer and the plates were sealed and incubated overnight at 4 °C. To increase the immunoreactivity of PrP^{Sc}, coated proteins were denatured *in situ*. 50 μ L of 8 M GdnHCl were added to each well and incubated for 10 minutes at room temperature. The ELISA plates were washed three times with TBST and blocked with 200 μ L of 3% BSA in TBS (20 mM Tris-HCl, 137 mM NaCl, pH 7.5) for 1 hour at 37 °C. After three washes with TBST, the plates were incubated with 100 μ L of anti-PrP antibody W226 (1.5 μ g/mL) in 1% BSA/TBS, at 37 °C for 2 hours. After several washes with TBST, 100 μ L of goat anti-mouse IgG Fab conjugated to HRP diluted 1:1000 in 1% BSA/TBS were added to

the plates and incubated at 37 °C for 1 hour. Again, plates were washed seven times with TBST, and then developed with 100 µL of 1-step TMB (3,3',5,5'- tetramethylbenzidine) Turbo ELISA HRP substrate (Pierce). The reaction was stopped by the addition of 100 µL of 2 M sulfuric acid to the plates. Absorbance at 450 nm was measured using a microplate reader (VersaMax, Molecular Devices). Dose-response curves and IC₅₀ values were computed using GraphPad Prism (Version 5.0, Demo Version).

2.2.7. Fluorescence microscopy analyses

N2a and ScN2a cells were seeded to semi-confluence on glass coverslips for 24 hours. The cells were fixed with 4% formaldehyde and simultaneously permeabilized with 0.1% of Triton-X 100 for 1 hour at RT. Then, cells were denatured with 6 M GndHCl for 10 minutes at RT. For PK treated cells, 20 µg/mL of PK was applied to coverslips for 15 minutes at 37 °C. Digestion was stopped with 2 mM PMSF for 15 minutes at RT. After blocking with 1% Normal Goat Serum (NGS) for 1 hour at RT, cells were incubated with 0.025% of Thioflavin T (ThT) in EtOH 80% for 8 minutes at RT. After two washes with 80% EtOH and water, the anti-PrP primary antibody (monoclonal antibody mAb W226) diluted 1:200 in 1% blocking solution was applied overnight at 4 °C. After two washes with PBS, incubation with fluorescently labeled secondary antibody diluted 1:1000 in blocking solution followed (Goat anti-mouse [GαMo]-AlexaFluor594, Life Technologies) for 1 hour at RT. Cells treated with compound **96** were incubated with 0.025% of drug in 80% EtOH for 8 minutes at RT. After several washes with PBS, coverslips were mounted using Vectashield mounting media (VECTOR Laboratories). Images were acquired with C1 confocal microscope (Nikon). FITC filter was used for detection of ThT and compound **96** staining, while PrP specific staining was acquired with 594 nm filter.

3. Results and Discussion

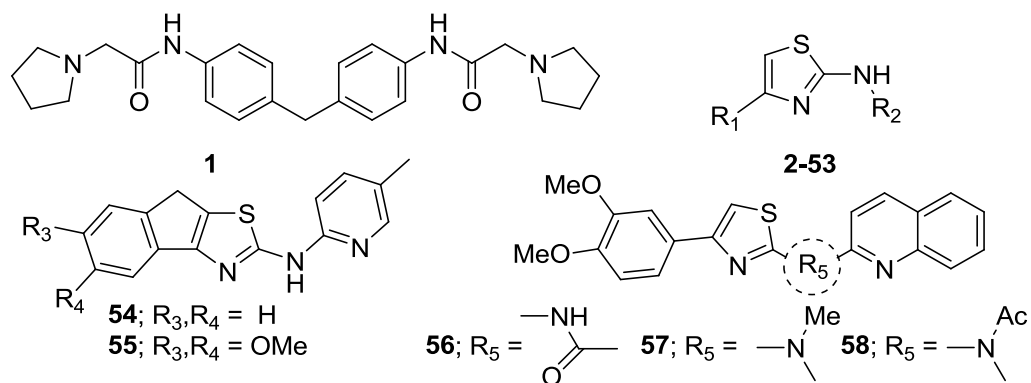
3.1. 3D-QSAR model generation

A combined computational protocol based on 3D-QSAR model and molecular docking calculations was set up to screen a proprietary chemical library for finding novel chemical entities possessing anti-prion activity.

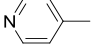
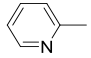
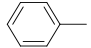
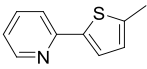
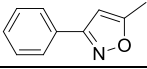
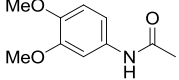
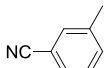
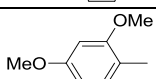
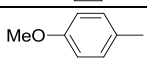
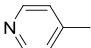
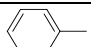
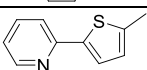
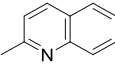
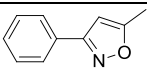

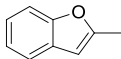
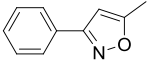
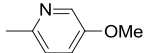
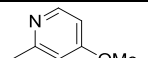
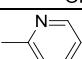
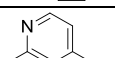
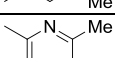
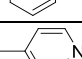
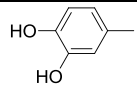
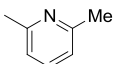
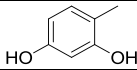
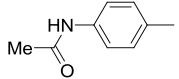
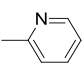
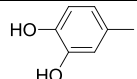
As the first step of our *in silico* protocol, we generated a 3D-QSAR model using pharmacophore based alignment as previously reported [41, 42, 45] adopting Phase software [57] that links the information of pivotal functional groups of the ligands with their biological activity. We have focused our attention on GN8 (**1**) [17] and different series of 2-aminothiazoles [19, 27, 58, 59] (**2-58**) for a total of 58 molecules (Table 1). This set of molecules was selected on the basis of the effective inhibition of the misfolding process following interaction with the same binding site. In particular, the selected compounds bind the PrP^C at the D-pocket formed by residues 156-162 and 180-210 in human PrP^C [17], a binding site already identified as key to be targeted for inhibiting the misfolding process, namely the conversion of PrP^C to PrP^{Sc} (Supplementary Figure 1). The functional activity is expressed as EC₅₀ [17].

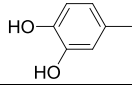
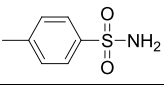
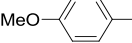
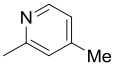
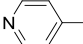
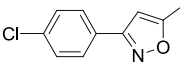
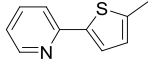
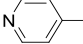
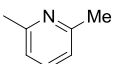
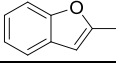
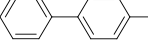
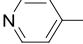
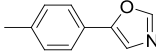
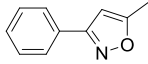
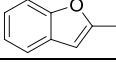
In the subsequent step of the computational protocol, an exhaustive conformational search for each ligand used in this study was performed employing MacroModel (see Supplementary Information for further details). This step was crucial to increase the quality of the alignment for the molecules chosen to generate the 3D-QSAR model as well as the reliability of the computational tool [40, 41, 44, 46, 60]. Accordingly, after the exhaustive conformational analysis of the selected ligands reported in Table 1, the generation of the 3D-QSAR model was started. As the first step to develop the 3D-QSAR model we generated a common features pharmacophore model taking into account the most active compounds included in the data set that consists of 58 molecules. Remarkably, the set of compounds selected for the development of the 3D-QSAR model spanned five orders of magnitude with reference to misfolding inhibition (Table 1) and the *in vitro* test for evaluating the anti-prion activity was performed by following the same protocol.

Table 1. Structures of the compounds used to derive the 3D-QSAR model with predicted activities as estimated by 3D-QSAR model.



Cpd	R ₁	R ₂	EC ₅₀ (nM)	Observed Activity	Predicted Activity
1 (GN8)^b	-	-	1350	5.87	5.67
2^a			3010	5.52	5.74
3^a			8200	5.09	4.95
4^a			1220	5.91	5.79
5^a			28000	4.55	4.43
6^b			6380	5.19	5.02
7^b			3940	5.40	5.35
8^b			15600	4.81	4.61
9^a			2530	5.60	5.59
10^a			1000	6.00	6.00
11^a			790	6.10	5.90
12^a			7290	5.14	5.18
13^b			1000	6.00	5.97
14^b			110	6.96	6.40
15^a			430	6.37	6.29
16^a			390	6.41	6.52
17^a			3030	5.52	5.59

18^b			1570	5.80	5.75
19^b			860	6.07	5.82
20^b			7880	5.10	5.25
21^b			1230	5.91	5.87
22^b			940	6.03	6.25
23^a			2440	5.61	5.62
24^b			2290	5.64	5.92
25^b			3130	5.50	5.68
26^a			340	6.47	6.28
27^a			310	6.51	6.23
28^a			3080	5.51	5.94
29^a			2010	5.70	5.78
30^b			800	6.10	6.28
31^a			8660	5.06	5.10
32^b			920	6.04	6.06
33^b			230	6.64	6.35
34^a			250	6.60	6.53
35^a			600	6.22	6.13
36^a			1270	5.90	6.06
37^b			820	6.09	6.16
38^a			4420	5.35	5.51
39^b			2500	5.60	5.54
40^a			3900	5.41	5.39
41^a			8500	5.07	5.01
42^b			10000	5.00	5.34

43^a			13500	4.87	4.82
44^a			1660	5.78	5.75
45^a			4950	5.30	5.52
46^b			850	6.07	6.07
47^a			1950	5.71	5.86
48^a			1000	6.00	5.78
49^a			1460	5.84	5.89
50^b			2290	5.90	5.73
51^a			124	6.91	7.02
52^a			57	7.24	7.34
53^a			228	6.64	6.57
54^b	-	-	2440	5.61	5.67
55^b	-	-	5590	5.25	5.53
56^a	-	-	8180	5.09	5.11
57^a	-	-	140	6.85	6.72
58^a	-	-	81	7.09	6.98

^aCompounds included in the training set; ^bCompounds included in the test set.

Compounds with $pEC_{50} > 6.5$ (**14**, **27**, **33**, **34**, **51-53**, **57**, **58**; Table 1 and Figure 2) were used to generate the common pharmacophore hypotheses, subsequently scored and ranked by Phase. Among the generated 3D model hypotheses, we selected AARRR.20, superposed in Figure 2A to compound **33**, highlighting five main features: two H-bond acceptor features (A), and three aromatic rings (R), underlining the structural requirements for interacting with the D-pocket of PrP^C. Figure 2B shows the inter-features distances of the hypothesis. This latter is in agreement with the recent findings indicating that planar conformations may be critical for anti-prion activity [61].

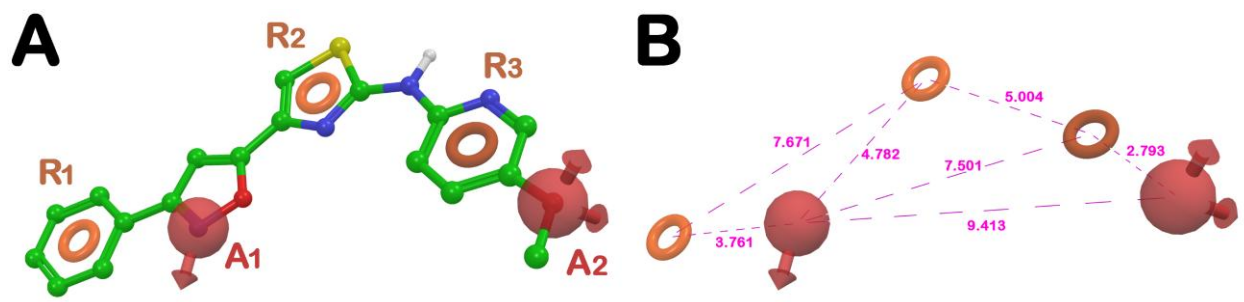


Figure 2. (A) Superposition of pharmacophore model AARRR.20 with one of the most active ligand in the set (33). Features of pharmacophore obtained by Phase are as follows: two hydrogen-bond acceptors (A₁ and A₂; represented by red vector) and three aromatic groups (R₁-R₃; orange rings). (B) Inter-features distances of the hypothesis.

Next, AARRR pharmacophore model was employed as alignment rule to derive the 3D-QSAR model. At this step the compounds were randomly subdivided in training (60%) and test sets (40%) (Table 1).

A

	PLS	r^{2a}	SD ^b	F ^c	P ^d	RMSE ^e	Q ^{2f}	Pearson R ^g
Hypothesis AARRR.20	1	0.534	0.464	37.9	6.15e-07	0.418	0.285	0.569
	2	0.779	0.324	56.4	3.24e-11	0.289	0.658	0.813
	3	0.881	0.242	76.4	2.05e-14	0.269	0.704	0.849
	4	0.932	0.186	102.2	5.01e-17	0.246	0.752	0.879
	5	0.953	0.157	117.4	2.51e-18	0.210	0.819	0.906

^a r^2 : value of r^2 of the regression; ^bSD: standard deviation of the regression; ^cF: variance ratio; ^dP: significance level of variance ratio; ^eRMSE: root-mean-square error; ^fQ²: value of Q² for the predicted activities; ^gR: R Pearson, R value for the correlation between the predicted and observed activity for the test set.

B

A scatter plot showing the relationship between experimental activity (x-axis) and phase predicted activity (y-axis). Both axes range from 4.0 to 7.5. A dashed diagonal line represents the identity line (y=x). Data points are represented by blue and pink dots, showing a strong positive correlation, with most points falling very close to the diagonal line.

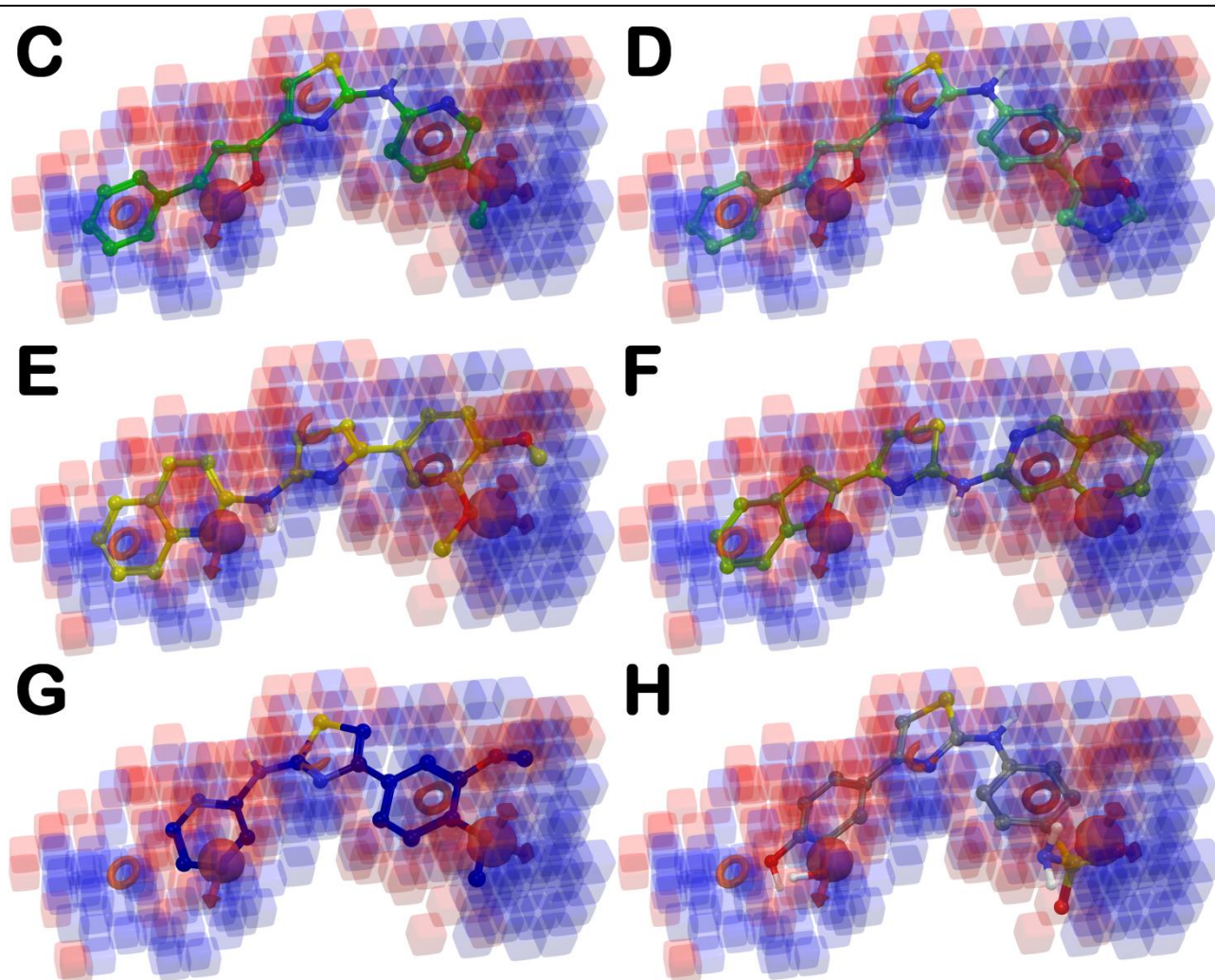


Figure 3. (A) Statistical parameters of the 3D-QSAR model; (B) Scatter plot for the predicted (phase predicted activity) and observed (experimental activity) pEC₅₀ values (M) as calculated by the 3D-QSAR model applied to the training set (blue) and test set compounds (red purple); (C-H) Superposition of highly active compounds **33** (C) and **52** (D), moderately actives **15** (E) and **32** (F) and two of the less actives compounds **8** (G) and **43** (H) with the 3D-QSAR model. Pictures were generated by means of Maestro.

Models containing one up to five PLS factors were generated (statistical parameters are reported in Figure 3A). The preferred model utilized five PLS factors. The high correlation and cross-validated correlation coefficients ($r^2 = 0.953$ and $Q^2 = 0.819$, respectively) together with the high Pearson R

value (R-Pearson = 0.906), led to a close correspondence between predicted and experimental EC₅₀ values, indicative for a robust and predictive model.

A scatter plot of experimental versus predicted activities was generated (Figure 3B), and EC₅₀ values were reliably predicted for both training and test set molecules (Table 1). These features, along with the low RMSE and SD, the large F value and the small variance ratio (P), supported the significance of the approach.

The 3D-QSAR results were visualized using 3D plots of the crucial volume elements occupied by ligands. The 3D plot representation of the model as a whole, superimposed to highly (**33,52**), moderate (**15,32**), and less active derivatives (**8,43**) is depicted in Figure 3 (Panel C-H, respectively). In this representation blue and red cubes specify positive and negative coefficients, respectively, that are volumes in which the occupying atoms of the ligands cause an increase or a decrease of activity. Notably, compounds **33** and **52** (Figure 3C and 3D, respectively) as well as highly active compounds, showing the greatest anti-prion activity, mainly lodge in the blue regions, while the less active derivatives such as **8** and **43** (Figure 3G and 3H, respectively) mainly lodge in the red regions.

3.1.1. *In silico* 3D-QSAR model validation

a) External test set

After the generation of the 3D-QSAR model an early *in silico* validation was performed by using an external test set selected from the literature [61] (**59-88**; Supplementary Table 1) and not used for generating the computational model. This set was composed of 30 compounds, with different potencies of PrP^C misfolding inhibition. As reported in Supplementary Table 1, our model was reasonably efficient in estimating the anti-prion activity of this set of compounds. In the scatter plot depicted in Supplementary Figure 2, the experimental and predicted pEC₅₀ values of these compounds are also displayed, providing a correlation coefficient comparable with that found for the internal cross-

validation (Q^2 in Figure 3A). This result furnishes further evidence that the correlation shown by the model was not accidental.

b) Decoys

In order to confirm the predictive power of the developed 3D-QSAR model, we have used a decoys set. This procedure is commonly used to evaluate the ability of computational models to discriminate between active or inactive molecules [40, 46, 62-64]. Starting from the active compounds herein presented (**14**, **27**, **33**, **34**, **51-53**, **57**, **58**; Table 1) and a series of related aminothiazoles employed in the external tests (**59-69**, **81-86**; Supplementary Table 1) and not used for generating the 3D-QSAR model (a complete list of active molecules for generation decoys was provided in Supplementary Table 2), we selected a total of 26 actives. From this latter set, DUD-E generated 1550 decoys. Next, after an appropriate preparation of decoys, we have combined them with the active molecules (*A*) for a total of 1576 compounds (*D*) to perform a virtual screening using the 3D-QSAR model (see Supplementary Information for further details).

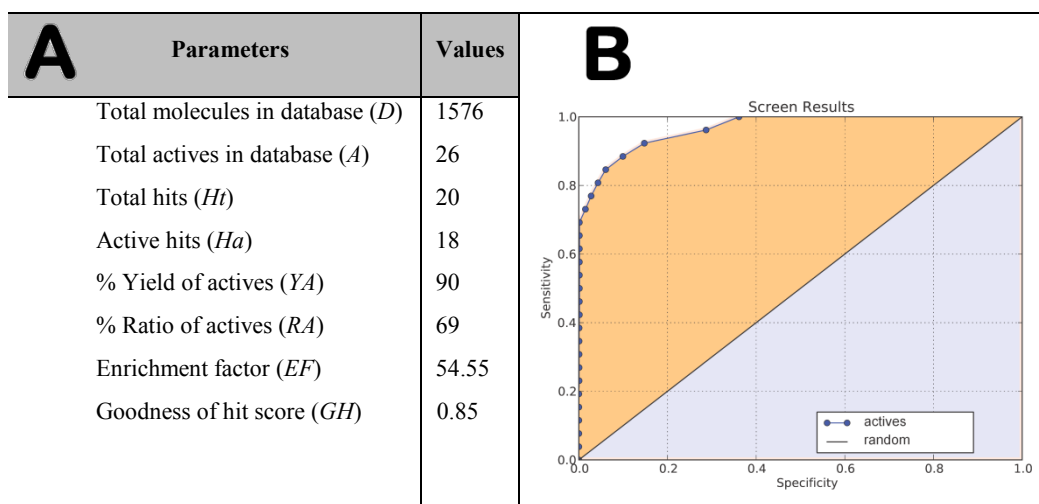


Figure 4. (A) *EF* and *GH* scores obtained by the application of 3D-QSAR model in a database screening; (B) ROC curve generated from database screening.

The database screening results showed that the top twenty ranked compounds were considered as hits (*Ht*). This value could represent a reasonable number of molecules to purchase after a virtual screening. Among these, 18 compounds (*Ha*) were from the 26 known inhibitors. Accordingly, the *EF* was calculated to be 54.55, which means that is about 54 times more probable to identify active compounds from databases than expected by chance. The calculated *GH* score value of 0.85, greater than 0.5 indicates a good reliability of the model (Figure 4A).

In addition, ROC curve was also used to estimate the performance of 3D-QSAR models. ROC curve can be used to assess the balance between model sensitivity (capability to discover true positives) and specificity (capability to avoid false positives) [48, 65]. The 1576 compounds in the validation database were ranked according to their predicted activity values as estimated by the 3D-QSAR model. The ROC score (AUC) provides a concrete way to measure the overall performance of the model. The closer the ROC score is to 1.0, the better the model is at distinguishing active compounds from inactive ones. ROC curve analysis of our developed 3D-QSAR model yielded a AUC score of 0.95 (Figure 4B). The *in silico* validation by using the above-described methods provided strong confidence on our computational tool, suggesting that the developed 3D-QSAR model had a rationale for virtual screening and it could be successfully employed to find novel chemical entities preventing the misfolding of PrP^C.

3.1.2. Virtual Screening

The 3D-QSAR model was subjected to a prospective experimental validation. An *in silico* database screening was executed to validate the newly developed computational approach, with the aim to discover new scaffolds with anti-prion properties [40, 41, 44]. For this purpose, the 3D-QSAR model was applied as the first fast filter to screen our proprietary database containing over 2,500 biologically active compounds. The use of a small library but also characterized by a good chemical diversity allowed us to test and experimentally validate our computational protocol in a short time. The library is

highly enriched with drug-like compounds encompassing a significant diversity of chemical scaffolds, ranging from four-, five-, six-, seven-membered heterocycles, bicyclic and tricyclic structures, to chiral compounds, peptides, peptidomimetics, metal ion binding and drug-like electrophilic compounds (for covalent enzyme inhibition). Moreover, our library has been previously used in virtual screening campaigns and employed in 3D-QSAR studies, retrieving active molecules against different targets [40, 66, 67].

To select novel scaffolds with potential anti-prion activity, we have retained only the molecules able to match at least four out of five pharmacophore features, showing a predicted $pEC_{50} \geq 6$ (predicted activity lower than 1 μM). Moreover, racemic compounds not showing similar predicted activities (< 0.1 logarithmic scale) for both enantiomers, were deprioritized from further computational investigation. The query identified 142 compounds satisfying the introduced requirements (Figure 1).

3.1.3. Molecular Docking studies

Subsequently, in order to narrow down the number of the potential hits and for improving the reliability of the protocol, a stepwise post-search filtering protocol was applied. It is well established that ligand-based virtual screening usually involves only the application of a pharmacophore to perform a fast database search. On the other hand, several recent studies have shown that coupling pharmacophore-based virtual screening with docking filtration can significantly improve the probability of identification of suitable hit candidates [68-70]. Accordingly, such a choice allows combining the primary purpose of pharmacophore validation with that of hit identification. A total number of 142 compounds with satisfactory predicted activities according to our developed 3D-QSAR model was selected and submitted to a docking protocol in the D-pocket binding site to better predict their affinity for PrP^C. The crystal structure of human PrP^C (PDB ID 2LEJ [71]) after appropriate treatment (see Protein Preparation paragraph) was used for molecular docking studies. An active site radius of 8 Å was chosen from H187 (roughly representing the center of the binding site in hPrP^C). Compounds were

docked employing the program Glide (Glide version 5.7, Schrödinger, LLC, New York, NY, 2011) applying Glide extra precision (XP) method to evaluate and rank the compounds. Score values lower than -7.00 kcal/mol were coupled to a visual inspection to retrieve compounds with an appropriate binding mode according to the key interactions found for the active compounds into the D-pocket [27, 29]. The query identified 59 compounds.

3.1.4. Molecular properties prediction

Fifty-nine compounds were analyzed by means of QikProp application (QikProp, version 3.4, Schrödinger, LLC, New York, NY, 2011) implemented in Maestro suite (Maestro, version 9.2, Schrödinger, LLC, New York, NY, 2011). This step was performed to select only molecules predicted to have satisfactory membrane permeability (QPPCaco-2 and QPPMDCK models > 200) and lipophilicity (QPlogP), including capability to cross the BBB (QPlogBB > -1.5). The potential interaction with *h*ERG (QPlogHERG) was also evaluated by *in silico* prediction. Compounds not showing these parameters in the appropriate range recommended by QikProp user manual were not considered for further evaluation. Furthermore, the resulting compounds were evaluated for their potential capability to behave as Pan Assay Interference Compounds (PAINS). This calculation was performed by means of FAFDrugs3.0 (<http://www.fafdrugs3.mti.univ-paris-diderot.fr> access date January 2016) [72]. Starting from 59 compounds, 16 were predicted to possess anti-prion activity and physico-chemicals properties suitable for BBB permeability (QPlogBB). Remarkably, the compounds filtered for PAINS indicated that none of them contain sub-structural features that would label them as “frequent hitters” in high throughput screens. Among the 16 molecule identified, compounds **89-104** [51-56] matched four out of five pharmacophore features, while compounds **96-98** matched all five pharmacophore features (Supplementary Table 3).

3.2. Biological Evaluation

Fourteen compounds were biologically evaluated for inhibition of the misfolding of PrP^C (compounds **91** and **92** were not available in appropriate amount for *in vitro* testing).

3.2.1. Effect of selected compounds on cell viability

The first step of the biological investigation was the assessment of toxicity of selected compounds by MTT assay (Table 2). Treatment of ScN2a cells with selected compounds at different doses (0.1 μ M; 1 μ M; 10 μ M) did not significantly modify cell viability with the exclusion of compounds **89,90** and **97** (Table 2). These latter were deprioritized from the assessment of PrP^{Sc} inhibition, since they showed a toxicity higher than 20% at a concentration of 1 μ M [73].

Table 2. Percentage of viable cells after treatment with 0.1 μ M, 1 μ M and 10 μ M of each compound measured by MTT assay.

Compound	0.1 μ M (%)	1 μ M (%)	10 μ M (%)
89	-	0.7	-
90	-	76.9	-
93	96.8 \pm 6.8	88.5 \pm 5.5	71.41 \pm 7.6
94	78.9 \pm 6.7	81.9 \pm 2.9	80.7 \pm 8.9
95	93.9 \pm 1.3	84.8 \pm 7.6	83.8 \pm 6.8
96	107.4 \pm 7.8	96.3 \pm 10.1	83.3 \pm 1.7
97	92.6 \pm 3.5	88.2 \pm 10.0	45.4 \pm 7.6
98	72.6 \pm 3.9	89.3 \pm 4.1	67.1 \pm 11.7
99	92.3 \pm 5.3	88.3 \pm 4.5	87.0 \pm 2.0
100	96.7 \pm 9.9	98.6 \pm 5.4	86.5 \pm 5.0
101	94.4 \pm 1.6	98.5 \pm 6.3	83.2 \pm 3.4
102	103.9 \pm 4.8	98.6 \pm 16.8	75.64 \pm 2.6
103	87.7 \pm 6.3	92.6 \pm 7.5	72.9 \pm 5.2
104	87.6 \pm 4.4	94.8 \pm 6.5	90.9 \pm 8.0
Ctrl	100	100	100

ScN2a cells were cultured in MEM and plated into 96-well plates (2.5×10^4 cell/mL). The compounds were dissolved in DMSO (100%) and diluted in EtOH. Test compounds were added and cells were incubated for 5 days at 37 °C, 5% CO₂. Values are expressed as mean \pm SD of three independent experiments.

3.2.2. Inhibition of PrP^{Sc} replication

Compounds showing no cytotoxic effect were then evaluated in prion-infected cells to quantify the formation of misfolded protein. The ability of compounds to reduce PrP^{Sc} levels in RML-infected N2a cells was determined by Western blot densitometric analysis. Relative amount of PK-resistant PrP^{Sc} was measured in ScN2a cell lysates after treatment with compounds of the library resulted not toxic in the cell viability assay. The majority of the compounds turned out to have mild anti-prion activity in a nontoxic range of concentrations. Western blot analysis of treated samples compared to untreated and mock-treated controls revealed that most of the compounds were able to reduce the amount of PrP^{Sc} at 10 μ M concentration. Indeed, nine compounds out of eleven reduced the level of PrP^{Sc} by more than 40% at the higher concentration tested (Table 3). Moreover, treatment of non-infected N2a cells revealed that none of the compounds had an effect on PrP^C levels (data not shown).

Table 3. Effect of test compounds on PrP^{Sc} level in ScN2a cells. ScN2a cells were incubated with each compound for 5 days.

Compound	0.1 μ M (%)	1 μ M (%)	10 μ M (%)
93	105%	86%	35%
94	88%	79%	72%
95	88%	77%	13%
96	76%	35%	9%
98	104%	131%	30%
99	90%	78%	27%
100	137%	100%	29%
101	178%	131%	30%
102	128%	144%	83%
103	76%	34%	31%
104	54%	47%	34%
Ctrl	100%	100%	100%

Cell lysates were digested with proteinase K (PK) and PrP^{Sc} content was detected by Western blot. Relative amount of PrP^{Sc} are calculated as ratio between PK-resistant PrP^{Sc} and total PrP levels, adjusting untreated controls to 100%. Values are expressed as mean \pm SD of three independent experiments.

Notably, nine out of eleven compounds reduced the level of PrP^{Sc} by more than 40% at the higher concentration tested. Among them, compound **96** (highlighted in grey background in Table 3) resulted to have the higher anti-prion activity. Indeed, the PrP^{Sc} signal was reduced by more than 60% in ScN2a

cells already after treatment with 1 μM concentration, being almost no longer detectable upon treatment with the higher concentration tested (10 μM) (Figures 5A, 5C). Following **96** treatment no significant variations of PrP^{C} levels were found in non-infected N2a cells (Figure 5B, 5D). This implies that the reduction of total PrP displayed in absence of PK digestion is caused primarily by the decrease of PrP^{Sc} rather than PrP^{C} . Effects of **96** treatment on cell viability and PrP content was also evaluated on ScGT1 and GT1 cells, and allowed to confirm the outcome reproducibility on a different cell model (data not shown). The IC_{50} of compound **96** is $1.6 \mu\text{M} \pm 0.05$ (Supplementary Figure 3).

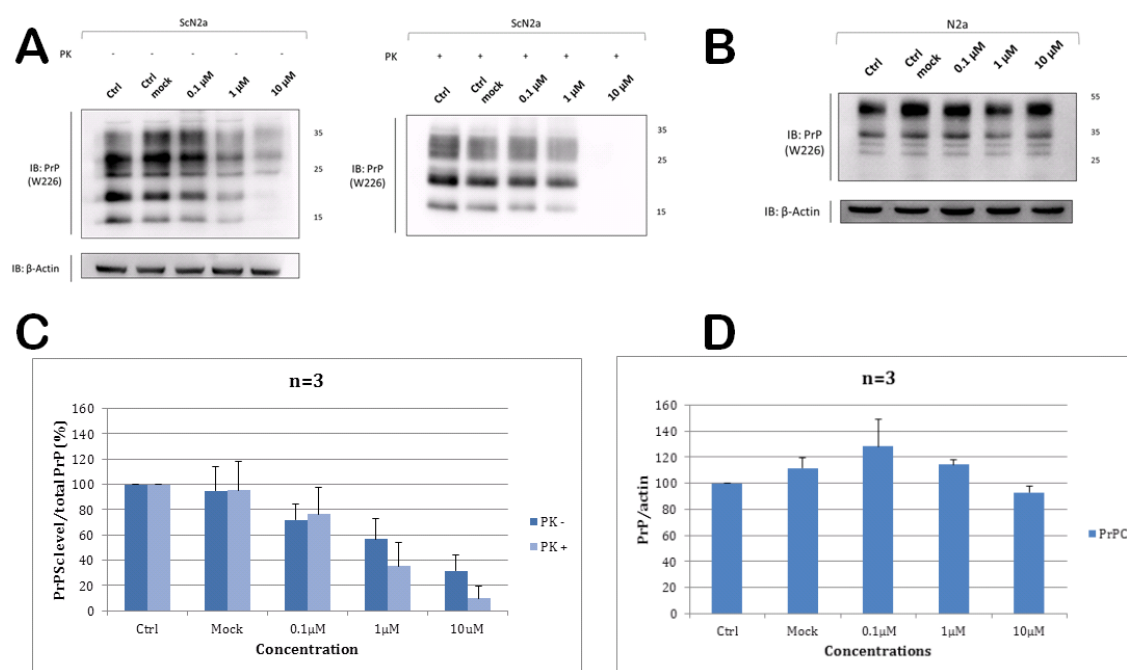


Figure 5. (A) Dose-dependent capacity of **96** to decrease PrP^{Sc} levels. Western blotting of ScN2a cell lysates depicting the presence or absence of prions following treatment with **96** before (left) or after (right) PK digestion. (B) Dose-dependent capacity of **96** to affect PrP^{C} levels on N2a cells. In both, cases anti-PrP Fab W226 was used. Relative amount of protein is calculated as ratio between PK-resistant PrP^{Sc} and total PrP levels (C), or PrP^{C} and actin (D), adjusting untreated controls to 100%. Values are expressed as mean \pm SD of three independent experiments. Strong reduction of PrP^{Sc} upon treatment with 10 μM of compound (C), without PrP^{C} level variation (D), was observed.

In Figure 6, the output belonging to our computational approach of one of the best hits is reported (**96**). In particular, the superposition between the 3D-QSAR model and **96** (Figure 6A) highlights that this hit matches all the pharmacophore features of the pharmacophore model and mainly lodges in the blue region of 3D-QSAR model (predicted pEC_{50} 6.34). Regarding the docking output the compound is able to tightly bind the D-pocket and this accounts for one of the best docking scores found by Glide XP method (XP score -7.58 kcal/mol) (Figure 6B).

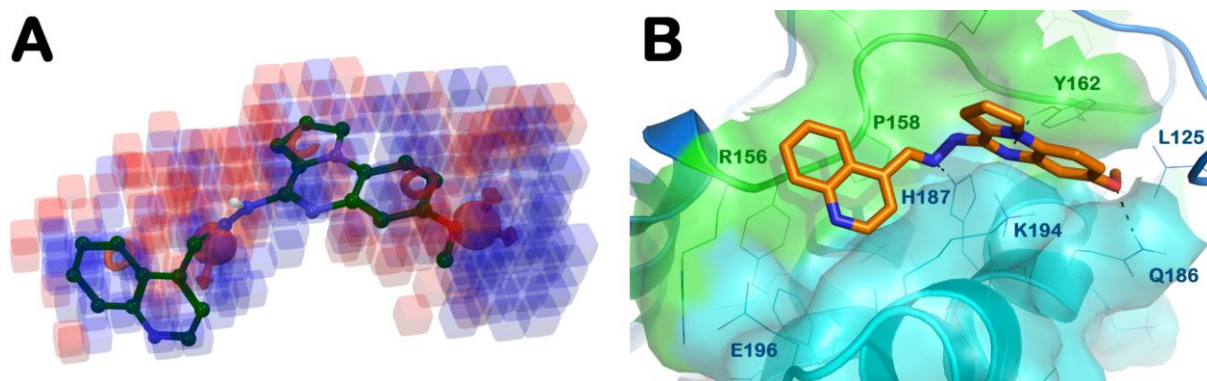


Figure 6. (A) Superposition between 3D-QSAR model and **96** as found by virtual screening procedure. The picture was generated by means of Maestro; (B) Best docked pose for compound **96** (sticks) into *hPrP^C* (PDB ID: 2LEJ). The key residues in the active site were represented by lines. In particular D-pocket is represented by solid surface. H-bonds were represented by black dotted lines. The hydrogens were omitted for the sake of clarity. The picture was generated by means of PyMOL (The PyMOL Molecular Graphics System, v1.6-alpha; Schrodinger, LLC, New York, 2013).

In particular, **96** interacts with H187 and Q186 by two H-bonds with the hydrazone moiety and with the oxygen belonging to the methoxy group, respectively. The pyrroloquinoxaline nucleus forms an H-bond with Y162. Notably, large hydrophobic contacts stabilize the binding mode. In fact, **96** can interact with P158 by its quinoline moiety while the pyrroloquinoxaline forms hydrophobic contacts with Y162, and a cation- π stacking with K194. The methyl belonging to the methoxy group is buried into a hydrophobic sub-pocket and establishes strong hydrophobic contacts with Y162 and L125. The

strong interactions with the residues located in the loop represented in green in Figure 6 (R156-Y162) can lead to a stabilization of the secondary structure, potentially preventing the progression of misfolding phenomena by precluding interaction of this region with other prion proteins (PrP^{Sc} and PrP^C). It is well established that this region is one of those involved in the early misfolding events. Based on this observation, molecules acting with this mechanism of action can potentially reduce the progression of PrP^C towards the pathological form PrP^{Sc} as highlighted by biological evaluation of the hit (Table 3 and Figure 5).

3.2.3. Detection of PrP^{Sc} aggregates

Building on the previous findings that pyrroloquinoxalines were able to bind amyloid fibrils and displayed an increase of their fluorescence upon binding [56], we also investigated the ability of most active compound **96** to bind and stain prion aggregates on ScN2a cell line. Due to large emission spectrum of compound **96**, fluorescent staining can be visualized with UV, FITC and TRITC filters. The binding of the compound to prion aggregates was compared to the staining obtained with ThT [74], which specifically binds β -sheet-rich deposits. Together with ThT staining, PrP specific signal was visualized. The fluorescence staining pattern of compound **96** on prion infected cells was very similar to that obtained with ThT and PrP specific immunostaining. The specificity of the binding to prion aggregates, and therefore the ability to discriminate between the abnormal, PK-resistant and β -sheet-rich PrP^{Sc} isoform and the normal, PK-sensitive PrP^C isoform, was confirmed by the absence of fluorescent signal on non-infected N2a cells (Figure 7).

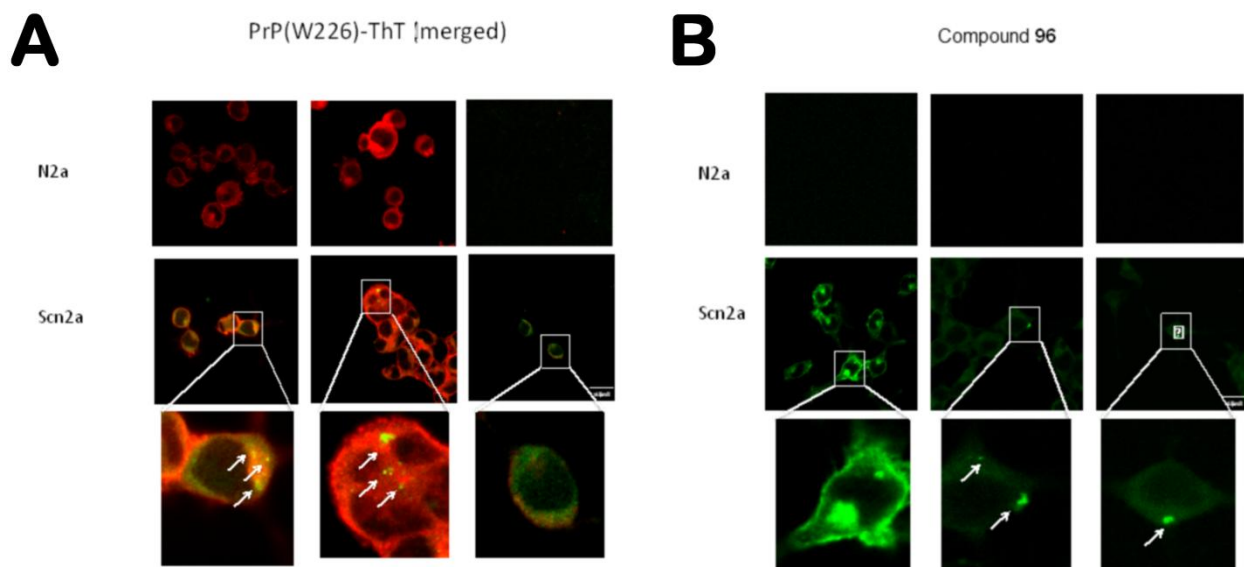


Figure 7. (A) Detection of PrP^{Sc} aggregates with anti-PrP antibody (W226) and ThT; **(B) 96** in ScN2a and N2a cells by intensity fluorescence (IF). Denaturation with 6 M guanidinium chloride (GndHCl) and PK digestion were performed. FITC filter was used for detection of ThT and compound **96** staining (green), while PrP specific staining was acquired with 594 nm filter (red). Scale bar 16 μm.

The data discussed so far clearly confirm the potential of **96** in reducing the formation of PrP^{Sc} indicating this molecule as a novel agent with remarkable anti-prion activity in cell models of the disease. Moreover, **96** demonstrated an interesting affinity for the β -sheet structure, irrespective of the specific protein originating it, combined with fluorescence properties that can be exploited for the visualization of aggregates. On the other hand, the observation that compound **96** is able to reduce PrP^{Sc} accumulation, but has not effect on A β fibrillogenesis (as detailed in our previous study) suggests a specific interaction of **96** with PrP^C [56].

4. Conclusion

In summary, we have presented a computational and biological protocol for the identification of novel potential therapeutic and diagnostic agents able to prevent the pathological transition of PrP^C to PrP^{Sc}.

For the prediction of anti-prion activity, a 3D-QSAR model was generated. Additionally, the potential affinity of the selected compounds for the binding site at the D-pocket of PrP^C was assessed by means of molecular docking simulation. The identified compounds were submitted to biological evaluation for validating our computational approach using enzyme-linked immunosorbent assay (ELISA) in prion-infected neuroblastoma cell lines (ScN2a). Satisfyingly, *in vitro* tests confirmed that nine out of eleven tested compounds showed anti-prion activity being able to prevent the misfolding events of PrP^C in the micro molar range. Cell viability on ScN2a cells assessed by means of MTT assay, highlighted the non-toxic profile of our retrieved hits. Among them, compound **96** was identified as a promising hit interfering with pathological misfolding of PrP^C to PrP^{Sc}. Moreover, **96** is able to bind and stain PrP^{Sc} aggregates in infected ScN2a. The combination of this interesting anti-prion cellular profile with a fluorescence imaging behavior, and the brain permeability previously demonstrated by the class of pyrroloquinoxaline hydrazones here described [56], which support our *in silico* predicted brain permeability of **96**, suggests that this compound could be considered as a prototypic tool the future development of diagnostic and therapeutic probes for prion diseases, as recently proposed for other classes of compounds, such as styrylquinoline against prion diseases [75] or other tools for Alzheimer's disease and related disorders [31, 76, 77].

Acknowledgement

This study was supported by grants from MIUR (Rome, grants PRIN-2010M2JARJ to G.C and G.L.). The authors wish to thank NatSynDrugs for technical support.

Supplementary data

Supplementary data associated to this article can be found at....

References

- [1] A. Kraus, B.R. Groveman, B. Caughey, Prions and the potential transmissibility of protein misfolding diseases, *Annual Review of Microbiology*, 67 (2013) 543-564.
- [2] E.D. Belay, Transmissible spongiform encephalopathies in humans, *Annual Review of Microbiology*, 53 (1999) 283-314.
- [3] S.B. Prusiner, Prions, *Proc Natl Acad Sci U S A*, 95 (1998) 13363-13383.
- [4] J. Singh, J.B. Udgaonkar, Molecular Mechanism of the Misfolding and Oligomerization of the Prion Protein: Current Understanding and Its Implications, *Biochemistry*, 54 (2015) 4431-4442.
- [5] C.Y. Acevedo-Morantes, H. Wille, The structure of human prions: from biology to structural models-considerations and pitfalls, *Viruses*, 6 (2014) 3875-3892.
- [6] R. Diaz-Espinoza, C. Soto, High-resolution structure of infectious prion protein: the final frontier, *Nat Struct Mol Biol*, 19 (2012) 370-377.
- [7] J.T. Jarrett, P.T. Lansbury, Jr., Seeding "one-dimensional crystallization" of amyloid: a pathogenic mechanism in Alzheimer's disease and scrapie?, *Cell*, 73 (1993) 1055-1058.
- [8] C.E. Mays, C. Soto, The stress of prion disease, *Brain Res*, 1648 (2016) 553-560.
- [9] M. Jucker, L.C. Walker, Self-propagation of pathogenic protein aggregates in neurodegenerative diseases, *Nature*, 501 (2013) 45-51.
- [10] S.B. Prusiner, Cell biology. A unifying role for prions in neurodegenerative diseases, *Science (New York, N Y)*, 336 (2012) 1511-1513.
- [11] S.B. Prusiner, Prion biology and diseases--laughing cannibals, mad cows, and scientific heresy, *Med Res Rev*, 16 (1996) 487-505.
- [12] A. Aguzzi, C. Sigurdson, M. Heikenwaelder, Molecular mechanisms of prion pathogenesis, *Annu Rev Pathol*, 3 (2008) 11-40.
- [13] H. Bueler, M. Fischer, Y. Lang, H. Bluethmann, H.P. Lipp, S.J. DeArmond, S.B. Prusiner, M. Aguet, C. Weissmann, Normal development and behaviour of mice lacking the neuronal cell-surface PrP protein, *Nature*, 356 (1992) 577-582.
- [14] A. Aguzzi, M. Polymenidou, Mammalian prion biology: one century of evolving concepts, *Cell*, 116 (2004) 313-327.
- [15] V. Perrier, A.C. Wallace, K. Kaneko, J. Safar, S.B. Prusiner, F.E. Cohen, Mimicking dominant negative inhibition of prion replication through structure-based drug design, *Proc Natl Acad Sci U S A*, 97 (2000) 6073-6078.
- [16] G. Mallucci, J. Collinge, Rational targeting for prion therapeutics, *Nat Rev Neurosci*, 6 (2005) 23-34.
- [17] K. Kuwata, N. Nishida, T. Matsumoto, Y.O. Kamatari, J. Hosokawa-Muto, K. Kodama, H.K. Nakamura, K. Kimura, M. Kawasaki, Y. Takakura, S. Shirabe, J. Takata, Y. Kataoka, S. Katamine, Hot spots in prion protein for pathogenic conversion, *Proc Natl Acad Sci U S A*, 104 (2007) 11921-11926.
- [18] C.R. Trevitt, J. Collinge, A systematic review of prion therapeutics in experimental models, *Brain*, 129 (2006) 2241-2265.
- [19] A. Gallardo-Godoy, J. Gever, K.L. Fife, B.M. Silber, S.B. Prusiner, A.R. Renslo, 2-Aminothiazoles as therapeutic leads for prion diseases, *J Med Chem*, 54 (2011) 1010-1021.
- [20] N.R. Cashman, B. Caughey, Prion diseases--close to effective therapy?, *Nat Rev Drug Discov*, 3 (2004) 874-884.
- [21] A. Aguzzi, T. O'Connor, Protein aggregation diseases: pathogenicity and therapeutic perspectives, *Nat Rev Drug Discov*, 9 (2010) 237-248.
- [22] V.L. Sim, Prion disease: chemotherapeutic strategies, *Infect Disord Drug Targets*, 12 (2012) 144-160.

- [23] D.A. Kocisko, N. Bertholet, R.A. Moore, B. Caughey, A. Vaillant, Identification of prion inhibitors by a fluorescence-polarization-based competitive binding assay, *Anal Biochem*, 363 (2007) 154-156.
- [24] C. Korth, B.C. May, F.E. Cohen, S.B. Prusiner, Acridine and phenothiazine derivatives as pharmacotherapeutics for prion disease, *Proc Natl Acad Sci U S A*, 98 (2001) 9836-9841.
- [25] I. Murakami-Kubo, K. Doh-Ura, K. Ishikawa, S. Kawatake, K. Sasaki, J. Kira, S. Ohta, T. Iwaki, Quinoline derivatives are therapeutic candidates for transmissible spongiform encephalopathies, *J Virol*, 78 (2004) 1281-1288.
- [26] M.L. Bolognesi, S. Bongarzone, S. Aulic, H.N. Ai Tran, F. Prati, P. Carloni, G. Legname, Rational approach to an antiprion compound with a multiple mechanism of action, *Future Med Chem*, 7 (2015) 2113-2120.
- [27] N.S. Pagadala, R. Perez-Pineiro, D.S. Wishart, J.A. Tuszynski, In silico studies and fluorescence binding assays of potential anti-prion compounds reveal an important binding site for prion inhibition from PrP(C) to PrP(Sc), *Eur J Med Chem*, 91 (2015) 118-131.
- [28] N.C. Ferreira, I.A. Marques, W.A. Conceicao, B. Macedo, C.S. Machado, A. Mascarello, L.D. Chiaradia-Delatorre, R.A. Yunes, R.J. Nunes, A.G. Hughson, L.D. Raymond, P.G. Pascutti, B. Caughey, Y. Cordeiro, Anti-prion activity of a panel of aromatic chemical compounds: in vitro and in silico approaches, *PLoS One*, 9 (2014) e84531.
- [29] J.W. Hyeon, J. Choi, S.Y. Kim, R.G. Govindaraj, K. Jam Hwang, Y.S. Lee, S.S. An, M.K. Lee, J.Y. Joung, K.T. No, J. Lee, Discovery of Novel Anti-prion Compounds Using In Silico and In Vitro Approaches, *Sci Rep*, 5 (2015) 14944.
- [30] Y.E. Karapetyan, G.F. Sferrazza, M. Zhou, G. Ottenberg, T. Spicer, P. Chase, M. Fallahi, P. Hodder, C. Weissmann, C.I. Lasmezas, Unique drug screening approach for prion diseases identifies tacrolimus and astemizole as antiprion agents, *Proc Natl Acad Sci U S A*, 110 (2013) 7044-7049.
- [31] S. Bongarzone, M. Staderini, M.L. Bolognesi, Multitarget ligands and theranostics: sharpening the medicinal chemistry sword against prion diseases, *Future Med Chem*, 6 (2014) 1017-1029.
- [32] E.A. Croes, Therapeutic approaches in treating Creutzfeldt-Jakob disease - what does the future hold?, *Expert Opin Pharmacother*, 5 (2004) 2391-2396.
- [33] C. Krammer, I. Vorberg, H.M. Schatzl, S. Gilch, Therapy in prion diseases: from molecular and cellular biology to therapeutic targets, *Infect Disord Drug Targets*, 9 (2009) 3-14.
- [34] M.L. Bolognesi, G. Legname, Approaches for discovering anti-prion compounds: lessons learned and challenges ahead, *Expert Opin Drug Discov*, 10 (2015) 389-397.
- [35] D.B. Berry, D. Lu, M. Geva, J.C. Watts, S. Bhardwaj, A. Oehler, A.R. Renslo, S.J. DeArmond, S.B. Prusiner, K. Giles, Drug resistance confounding prion therapeutics, *Proc Natl Acad Sci U S A*, 110 (2013) E4160-4169.
- [36] M. Manix, P. Kalakoti, M. Henry, J. Thakur, R. Menger, B. Guthikonda, A. Nanda, Creutzfeldt-Jakob disease: updated diagnostic criteria, treatment algorithm, and the utility of brain biopsy, *Neurosurgical Focus*, 39 (2015) E2.
- [37] F. Moda, P. Gambetti, S. Notari, L. Concha-Marambio, M. Catania, K.W. Park, E. Maderna, S. Suardi, S. Haik, J.P. Brandel, J. Ironside, R. Knight, F. Tagliavini, C. Soto, Prions in the urine of patients with variant Creutzfeldt-Jakob disease, *N Engl J Med*, 371 (2014) 530-539.
- [38] C.D. Orru, B.R. Groveman, A.G. Hughson, G. Zanusso, M.B. Coulthart, B. Caughey, Rapid and sensitive RT-QuIC detection of human Creutzfeldt-Jakob disease using cerebrospinal fluid, *Mbio*, 6 (2015).
- [39] G. Zanusso, S. Monaco, M. Pocchiari, B. Caughey, Advanced tests for early and accurate diagnosis of Creutzfeldt-Jakob disease, *Nat Rev Neurol*, 12 (2016) 325-333.

- [40] S. Brogi, M. Brindisi, B.P. Joshi, S. Sanna Coccone, S. Parapini, N. Basilico, E. Novellino, G. Campiani, S. Gemma, S. Butini, Exploring clotrimazole-based pharmacophore: 3D-QSAR studies and synthesis of novel antiplasmodial agents, *Bioorg Med Chem Lett*, 25 (2015) 5412-5418.
- [41] S. Brogi, P. Papazafiri, V. Roussis, A. Tafi, 3D-QSAR using pharmacophore-based alignment and virtual screening for discovery of novel MCF-7 cell line inhibitors, *Eur J Med Chem*, 67 (2013) 344-351.
- [42] S. Pasquini, C. Mugnaini, A. Ligresti, A. Tafi, S. Brogi, C. Falciani, V. Pedani, N. Pesco, F. Guida, L. Luongo, K. Varani, P.A. Borea, S. Maione, V. Di Marzo, F. Corelli, Design, synthesis, and pharmacological characterization of indol-3-ylacetamides, indol-3-yloxoacetamides, and indol-3-ylcarboxamides: potent and selective CB2 cannabinoid receptor inverse agonists, *J Med Chem*, 55 (2012) 5391-5402.
- [43] M.P. Castelli, A. Casu, P. Casti, C. Lobina, M.A. Carai, G. Colombo, M. Solinas, D. Giunta, C. Mugnaini, S. Pasquini, A. Tafi, S. Brogi, G.L. Gessa, F. Corelli, Characterization of COR627 and COR628, two novel positive allosteric modulators of the GABA(B) receptor, *J Pharmacol Exp Ther*, 340 (2012) 529-538.
- [44] S. Brogi, F. Corelli, V. Di Marzo, A. Ligresti, C. Mugnaini, S. Pasquini, A. Tafi, Three-dimensional quantitative structure-selectivity relationships analysis guided rational design of a highly selective ligand for the cannabinoid receptor 2, *Eur J Med Chem*, 46 (2011) 547-555.
- [45] S. Gemma, S. Brogi, P.R. Patil, S. Giovani, S. Lamponi, A. Cappelli, E. Novellino, A. Brown, M.K. Higgins, K. Mustafa, T. Szeszak, A.G. Craig, G. Campiani, S. Butini, M. Brindisi, From (+)-epigallocatechin gallate to a simplified synthetic analogue as a cytoadherence inhibitor for *P. falciparum*, *RSC Advances*, 4 (2014) 4769-4781.
- [46] S. Brogi, S. Giovani, M. Brindisi, S. Gemma, E. Novellino, G. Campiani, M.J. Blackman, S. Butini, In silico study of subtilisin-like protease 1 (SUB1) from different *Plasmodium* species in complex with peptidyl-difluorostatones and characterization of potent pan-SUB1 inhibitors, *J Mol Graph Model*, 64 (2016) 121-130.
- [47] W.L. Jorgensen, D.S. Maxwell, J. TiradoRives, Development and testing of the OPLS all atom force field on conformational energetics and properties of organic liquids *J. Am. Chem. Soc.*, 118 (1996) 11225-11236.
- [48] N. Triballeau, F. Acher, I. Brabet, J.P. Pin, H.O. Bertrand, Virtual screening workflow development guided by the "receiver operating characteristic" curve approach. Application to high-throughput docking on metabotropic glutamate receptor subtype 4, *J Med Chem*, 48 (2005) 2534-2547.
- [49] T.A. Halgren, R.B. Murphy, R.A. Friesner, H.S. Beard, L.L. Frye, W.T. Pollard, J.L. Banks, Glide: a new approach for rapid, accurate docking and scoring. 2. Enrichment factors in database screening, *J Med Chem*, 47 (2004) 1750-1759.
- [50] R.A. Friesner, J.L. Banks, R.B. Murphy, T.A. Halgren, J.J. Klicic, D.T. Mainz, M.P. Repasky, E.H. Knoll, M. Shelley, J.K. Perry, D.E. Shaw, P. Francis, P.S. Shenkin, Glide: a new approach for rapid, accurate docking and scoring. 1. Method and assessment of docking accuracy, *J Med Chem*, 47 (2004) 1739-1749.
- [51] G. Campiani, C. Fattorusso, S. Butini, A. Gaeta, M. Agnusdei, S. Gemma, M. Persico, B. Catalanotti, L. Savini, V. Nacci, E. Novellino, H.W. Holloway, N.H. Greig, T. Belinskaya, J.M. Fedorko, A. Saxena, Development of molecular probes for the identification of extra interaction sites in the mid-gorge and peripheral sites of butyrylcholinesterase (BuChE). Rational design of novel, selective, and highly potent BuChE inhibitors, *J Med Chem*, 48 (2005) 1919-1929.
- [52] S. Butini, G. Campiani, M. Borriello, S. Gemma, A. Panico, M. Persico, B. Catalanotti, S. Ros, M. Brindisi, M. Agnusdei, I. Fiorini, V. Nacci, E. Novellino, T. Belinskaya, A. Saxena, C. Fattorusso,

Exploiting protein fluctuations at the active-site gorge of human cholinesterases: further optimization of the design strategy to develop extremely potent inhibitors, *J Med Chem*, 51 (2008) 3154-3170.

[53] S. Gemma, C. Camodeca, M. Brindisi, S. Brogi, G. Kukreja, S. Kunjir, E. Gabellieri, L. Lucantoni, A. Habluetzel, D. Taramelli, N. Basilico, R. Gualdani, F. Tadini-Buoninsegni, G. Bartolommei, M.R. Moncelli, R.E. Martin, R.L. Summers, S. Lamponi, L. Savini, I. Fiorini, M. Valoti, E. Novellino, G. Campiani, S. Butini, Mimicking the intramolecular hydrogen bond: synthesis, biological evaluation, and molecular modeling of benzoxazines and quinazolines as potential antimalarial agents, *J Med Chem*, 55 (2012) 10387-10404.

[54] S. Gemma, S. Giovani, M. Brindisi, P. Tripaldi, S. Brogi, L. Savini, I. Fiorini, E. Novellino, S. Butini, G. Campiani, M. Penzo, M.J. Blackman, Quinolyldhydrazones as novel inhibitors of *Plasmodium falciparum* serine protease PfSUB1, *Bioorg Med Chem Lett*, 22 (2012) 5317-5321.

[55] T. Bandiera, A.E. Buhl, D.B. Carter, J. Lansen, C. Pellerano, T.J. Raub, L. Savini, S.P. Tanis, Compounds and methods for diagnosing and treating amyloid-related conditions, in, Google Patents, 2002.

[56] S. Gemma, L. Colombo, G. Forloni, L. Savini, C. Fracasso, S. Caccia, M. Salmona, M. Brindisi, B.P. Joshi, P. Tripaldi, G. Giorgi, O. Taglialatela-Scafati, E. Novellino, I. Fiorini, G. Campiani, S. Butini, Pyrroloquinoxaline hydrazones as fluorescent probes for amyloid fibrils, *Org Biomol Chem*, 9 (2011) 5137-5148.

[57] S.L. Dixon, A.M. Smondyrev, E.H. Knoll, S.N. Rao, D.E. Shaw, R.A. Friesner, PHASE: a new engine for pharmacophore perception, 3D QSAR model development, and 3D database screening: 1. Methodology and preliminary results, *J Comput Aided Mol Des*, 20 (2006) 647-671.

[58] S. Ghaemmaghami, B.C. May, A.R. Renslo, S.B. Prusiner, Discovery of 2-aminothiazoles as potent antiprion compounds, *J Virol*, 84 (2010) 3408-3412.

[59] B.M. Silber, S. Rao, K.L. Fife, A. Gallardo-Godoy, A.R. Renslo, D.K. Dalvie, K. Giles, Y. Freyman, M. Elepano, J.R. Gever, Z. Li, M.P. Jacobson, Y. Huang, L.Z. Benet, S.B. Prusiner, Pharmacokinetics and metabolism of 2-aminothiazoles with antiprion activity in mice, *Pharm Res*, 30 (2013) 932-950.

[60] S. Durdagi, H.J. Duff, S.Y. Noskov, Combined receptor and ligand-based approach to the universal pharmacophore model development for studies of drug blockade to the hERG1 pore domain, *J Chem Inf Model*, 51 (2011) 463-474.

[61] Z. Li, B.M. Silber, S. Rao, J.R. Gever, C. Bryant, A. Gallardo-Godoy, E. Dolgih, K. Widjaja, M. Elepano, M.P. Jacobson, S.B. Prusiner, A.R. Renslo, 2-Aminothiazoles with improved pharmacotherapeutic properties for treatment of prion disease, *ChemMedChem*, 8 (2013) 847-857.

[62] O. Dror, D. Schneidman-Duhovny, Y. Inbar, R. Nussinov, H.J. Wolfson, Novel approach for efficient pharmacophore-based virtual screening: method and applications, *J Chem Inf Model*, 49 (2009) 2333-2343.

[63] R.C. Braga, C.H. Andrade, Assessing the performance of 3D pharmacophore models in virtual screening: how good are they?, *Curr Top Med Chem*, 13 (2013) 1127-1138.

[64] S. Krishna, D.K. Singh, S. Meena, D. Datta, M.I. Siddiqi, D. Banerjee, Pharmacophore-based screening and identification of novel human ligase I inhibitors with potential anticancer activity, *J Chem Inf Model*, 54 (2014) 781-792.

[65] W. Zhao, K.E. Hevener, S.W. White, R.E. Lee, J.M. Boyett, A statistical framework to evaluate virtual screening, *BMC Bioinformatics*, 10 (2009) 225.

[66] M. Brindisi, S. Brogi, N. Relitti, A. Vallone, S. Butini, S. Gemma, E. Novellino, G. Colotti, G. Angiulli, F. Di Chiaro, A. Fiorillo, A. Ilari, G. Campiani, Structure-based discovery of the first non-covalent inhibitors of *Leishmania major* trypanothione peroxidase by high throughput docking, *Sci Rep*, 5 (2015) 9705.

- [67] M. Brindisi, S. Brogi, S. Giovani, S. Gemma, S. Lamponi, F. De Luca, E. Novellino, G. Campiani, J.D. Docquier, S. Butini, Targeting clinically-relevant metallo-beta-lactamases: from high-throughput docking to broad-spectrum inhibitors, *J Enzyme Inhib Med Chem*, (2016) 1-12.
- [68] S. Brogi, M. Kladi, C. Vagias, P. Papazafiri, V. Roussis, A. Tafi, Pharmacophore modeling for qualitative prediction of antiestrogenic activity, *J Chem Inf Model*, 49 (2009) 2489-2497.
- [69] M. Pappalardo, N. Shachaf, L. Basile, D. Milardi, M. Zeidan, J. Raiyn, S. Guccione, A. Rayan, Sequential application of ligand and structure based modeling approaches to index chemicals for their hH4R antagonism, *PLoS One*, 9 (2014) e109340.
- [70] M.L. Peach, M.C. Nicklaus, Combining docking with pharmacophore filtering for improved virtual screening, *J Cheminform*, 1 (2009) 6.
- [71] I. Biljan, G. Ilc, G. Giachin, A. Raspadori, I. Zhukov, J. Plavec, G. Legname, Toward the molecular basis of inherited prion diseases: NMR structure of the human prion protein with V210I mutation, *J Mol Biol*, 412 (2011) 660-673.
- [72] D. Lagorce, O. Sperandio, J.B. Baell, M.A. Miteva, B.O. Villoutreix, FAF-Drugs3: a web server for compound property calculation and chemical library design, *Nucleic Acids Res*, 43 (2015) W200-207.
- [73] G. Poncet-Montange, S.J. St Martin, O.V. Bogatova, S.B. Prusiner, B.K. Shoichet, S. Ghaemmaghami, A survey of antiprion compounds reveals the prevalence of non-PrP molecular targets, *J Biol Chem*, 286 (2011) 27718-27728.
- [74] R. Khurana, C. Coleman, C. Ionescu-Zanetti, S.A. Carter, V. Krishna, R.K. Grover, R. Roy, S. Singh, Mechanism of thioflavin T binding to amyloid fibrils, *J Struct Biol*, 151 (2005) 229-238.
- [75] M. Staderini, S. Aulic, M. Bartolini, H.N. Tran, V. Gonzalez-Ruiz, D.I. Perez, N. Cabezas, A. Martinez, M.A. Martin, V. Andrisano, G. Legname, J.C. Menendez, M.L. Bolognesi, A Fluorescent Styrylquinoline with Combined Therapeutic and Diagnostic Activities against Alzheimer's and Prion Diseases, *ACS Med Chem Lett*, 4 (2013) 225-229.
- [76] S. Aulic, M.L. Bolognesi, G. Legname, Small-molecule theranostic probes: a promising future in neurodegenerative diseases, *Int J Cell Biol*, 2013 (2013) 150952.
- [77] M.L. Bolognesi, A. Gandini, F. Prati, E. Uliassi, From Companion Diagnostics to Theranostics: A New Avenue for Alzheimer's Disease?, *J Med Chem*, 59 (2016) 7759-7770.

Supplementary Material - For Publication Online

[Click here to download Supplementary Material - For Publication Online: supplementary_file_rev.docx](#)

Mol Files

[Click here to download Mol Files: compound96.mol](#)

3D molecular models (.PDB, .PSE, .MOL, .MOL2)

[Click here to download 3D molecular models \(.PDB, .PSE, .MOL, .MOL2\): PrP_2LEJ_compound_96.pse](#)